

general Pol II transcription factors^{7,20,25,26}. All protein fractions were dialysed against buffer B (25 mM Tris-HCl, pH 7.9, 50 mM KCl, 0.5 mM dithiothreitol, 0.1 mM EDTA and 20% glycerol (v/v)). 25- μ l reactions contained either 25 ng 17M/5pAL7 and pG1 (ref. 5) or 100 ng pTEF(Δ -138) or pTEF(Δ -138_{TATA})¹⁵, with aliquots of TFTC, TFIID β and recombinant TBP⁵. Where indicated, 200 ng purified anti-TBP monoclonal antibody 1C2 was also included in the reactions before the other factors were added. GAL-VP16-activated transcription was performed as described⁵. After the preincubation steps (30 min), transcription was initiated by addition of nucleoside triphosphates to 0.5 mM and MgCl₂ to 5 mM. Transcriptions were incubated at 25 °C for 45 min. Correctly initiated transcripts from the different promoters were analysed by quantitative S1 nuclease analysis^{15,27}.

DNase I footprinting. DNase I footprinting was performed as described^{18,19}. The labelled AdMLP-containing probes were amplified by polymerase chain reaction on either the 17M5/pAL7 (ref. 28) (Fig. 3a) or the pM677 (ref. 29) (Fig. 3b) templates. For the footprinting experiments, ten times more TBP, TFIID β , and TFTC was used than in the transcription reactions.

Received 4 December 1997; accepted 6 March 1998.

- Zawel, L. & Reinberg, D. Common themes in assembly and function of eukaryotic transcription complexes. *Annu. Rev. Biochem.* **64**, 533–561 (1995).
- Roeder, R. G. The role of general initiation factors in transcription by RNA polymerase II. *Trends Biochem. Sci.* **21**, 327–335 (1996).
- Verrijzer, C. P. & Tjian, R. TAFs mediate transcriptional activation and promoter selectivity [see comments]. *Trends Biochem. Sci.* **21**, 338–342 (1996).
- Chang, M. & Jaehning, J. A. A multiplicity of mediators: alternative forms of transcription complexes communicate with transcriptional regulators. *Nucleic Acids Res.* **25**, 4861–4865 (1997).
- Brou, C. *et al.* Distinct TFIID complexes mediate the effect of different transcriptional activators. *EMBO J.* **12**, 489–499 (1993).
- Jacq, X. *et al.* Human TAFII30 is present in a distinct TFIID complex and is required for transcriptional activation by the estrogen receptor. *Cell* **79**, 107–117 (1994).
- Bertolotti, A., Lutz, Y., Heard, D. J., Chambon, P. & Tora, L. hTAFII68 a novel RNA/SSDNA-binding protein with homology to the pro-oncogene proteins TLS/FUS and EWS is associated with both TFIID and RNA polymerase II. *EMBO J.* **15**, 5022–5031 (1996).
- Mengus, G. *et al.* Cloning and characterization of hTAFII118, hTAFII20 and hTAFII28; three subunits of the human transcription factor TFIID. *EMBO J.* **14**, 1520–1531 (1995).
- Lescure, A. *et al.* The N-terminal domain of human TATA-binding protein plays a role in transcription from TATA-containing RNA polymerase II and III promoters. *EMBO J.* **13**, 1166–1175 (1994).
- Usheva, A. & Shenk, T. TATA-binding protein-independent initiation: YY1, TFIIB, and RNA polymerase II direct basal transcription on supercoiled template DNA. *Cell* **76**, 1115–1121 (1994).
- Timmers, H. T. M., Meyers, R. E. & Sharp, P. A. Composition of transcription factor B-TFIID. *Proc. Natl Acad. Sci. USA* **89**, 8140–8144 (1992).
- Van der Knaap, J. A., Willem Borst, J., van der Vliet, P. C., Gentz, R. & Timmers, H. T. M. Cloning of the cDNA for the TATA-binding protein-associated factor₁₇₀ subunit of transcription factor B-TFIID reveals homology to global transcription regulators in yeast and *Drosophila*. *Proc. Natl Acad. Sci. USA* **94**, 11827–11832 (1997).
- Hansen, S. K., Takada, S., Jacobson, R. H., Lis, J. T. & Tjian, R. Transcription properties of a cell type specific TATA-binding protein, TRF. *Cell* **91**, 71–83 (1997).
- Crowley, T. E., Hoey, T., Liu, J. K., Jan, Y. N., Jan, L. Y. & Tjian, R. A new factor related to TATA-binding protein has highly restricted expression patterns in *Drosophila*. *Nature* **361**, 557–561 (1993).
- Boam, D. S., Davidson, I. & Chambon, P. A TATA-less promoter containing binding sites for ubiquitous transcription factors mediates cell type-specific regulation of the gene for transcription enhancer factor-1 (TEF-1). *J. Biol. Chem.* **270**, 487–494 (1995).
- Nakajima, N., Horikoshi, M. & Roeder, R. G. Factors involved in specific transcription by mammalian RNA polymerase II: purification, genetic specificity, and TATA box-promoter interactions of TFIID. *Mol. Cell. Biol.* **8**, 4028–4040 (1988).
- Pugh, B. F. & Tjian, R. Transcription from a TATA-less promoter requires a multisubunit TFIID complex. *Genes Dev.* **5**, 1935–1945 (1991).
- Purnell, B. A., Emanuel, P. A. & Gilmour, D. S. TFIID sequence recognition of the initiator and sequences further downstream in *Drosophila* class II genes. *Genes Dev.* **8**, 830–842 (1994).
- Oelgeschlager, T., Chiang, C. M. & Roder, R. G. Topology and reorganization of a human TFIID-promoter complex. *Nature* **382**, 735–738 (1996).
- Dubrovskaya, V. *et al.* Distinct domains of hTAF₁₁₀₀ are required for functional interaction with transcription factor TFIIF β (RAP30) and incorporation into the TFIID complex. *EMBO J.* **15**, 3702–3712 (1996).
- Ruppert, S. & Tjian, R. Human TAFII250 interacts with RAP74: implications for RNA polymerase II initiation. *Genes Dev.* **9**, 2747–2755 (1995).
- Hisatake, K. *et al.* Evolutionary conservation of human TATA-binding-polypeptide-associated factors TAFII31 and TAFII80 and interactions of TAFII80 with other TAFs and with general transcription factors. *Proc. Natl Acad. Sci. USA* **92**, 85–89 (1995).
- Lavigne, A. C. *et al.* Multiple interactions between hTAFII55 and other TFIID subunits. Requirements for the formation of stable ternary complexes between hTAFII55 and the TATA-binding protein. *J. Biol. Chem.* **271**, 774–780 (1996).

- Lennon, G., Auffray, C., Polymeropoulos, M. & Soares, M. B. The I.M.A.G.E. Consortium: an integrated molecular analysis of genomes and their expression. *Genomics* **33**, 151–152 (1996).
- Gerard, M. *et al.* Purification and interaction properties of the human RNA polymerase B(II) general transcription factor BTF2. *J. Biol. Chem.* **266**, 20940–20945 (1991).
- De Jong, J. & Roeder, R. G. A single cDNA, hTFIIA/alpha, encodes both the p35 and p19 subunits of human TFIIA. *Genes Dev.* **7**, 2220–2234 (1993).
- Tora, L. *et al.* The human estrogen receptor has two independent nonacidic transcriptional activation functions. *Cell* **59**, 477–487 (1989).
- Brou, C. *et al.* Different TBP-associated factors are required for mediating the stimulation of transcription *in vitro* by the acidic transactivator GAL-VP16 and the two nonacidic activation functions of the estrogen receptor. *Nucleic Acids Res.* **21**, 5–12 (1993).
- Moncollin, V., Miyamoto, N. G., Zheng, X. M. & Egly, J. M. Purification of a factor specific for the upstream element of the adenovirus-2 major late promoter. *EMBO J.* **5**, 2577–2584 (1986).

Acknowledgements. We thank P. Chambon for support; J. C. Dantonel for help in identification and cloning of hTLF; E. Scheer for technical assistance; Y. Lutz for antibodies; D. Boam, V. Dubrovskaya, A. C. Lavigne, G. Mengus, I. Davidson and the IMAGE Consortium for reagents; H. T. M. Timmers for antibodies and for discussing unpublished results; A. Bertolotti for discussions; D. J. Heard for discussions and reading the manuscript; P. Eberling for peptide synthesis; the cell culture group for HeLa cells; R. Buchert, J.-M. Lafontaine and B. Boulay for illustrations; and A. Ozyhar for his contribution to the training of E.W. E.W. was supported by a fellowship from the Ministère de l'Enseignement Supérieur et de la Recherche. Research was supported by grants from the CNRS, the INSERM, the Hôpital Universitaire de Strasbourg, the Ministère de la Recherche et Technologie, the Fondation pour la Recherche Médicale and the Association pour la Recherche contre le Cancer.

Correspondence and requests for materials should be addressed to L.T. (e-mail: laszlo@titus.u-strasbg.fr).

corrections

Structure of the $\alpha\beta$ tubulin dimer by electron crystallography

Eva Nogales, Sharon G. Wolf & Kenneth H. Downing

Nature **391**, 199–203 (1998)

In this Letter, the numbers for the secondary structure elements involved in Taxol binding are incorrect (page 202, second-to-last paragraph of main text). The sentences giving the correct numbers are, “In our model, the C-3’ is near the top of helix H1 (that is, between β :15–25), and the C2 group near H6 and the H6–H7 loop (that is, between β :212–222). The main interaction of the taxane ring is at L275, at the beginning of the B7–H9 loop.” □

Spatial and temporal organization during cardiac fibrillation

Richard A. Gray, Arkady M. Pertsov & José Jalife

Nature **392**, 75–78 (1998)

The x-axis of Fig. 1d was mislabelled: the frequency values should instead read 0, 10, 20, 30, 40 Hz. □

bootstrap replicates. ML analyses of these two trees showed that they are not significantly different.

Effects of long-branch taxa. To identify taxa with long apparent branch lengths, we performed a four-taxon NJ analysis (using gamma-corrected Kimura distances) using *Tripedalia* (a diploblast), *Antedon* (a deuterostome) and *Glycera* (a protostome) with each nematode taxon in turn. We recorded the inferred distance from the protostome–nematode node to the nematode taxon. MP distances were derived from the phylogeny presented in Fig. 1. These long-branch-length taxa often have extreme base-composition biases, but not all taxa with extreme base compositions have long branch lengths (for example, *Brugia* has an AT content of 79% but one of the shorter inferred branch lengths). NJ and MP analyses were re-performed with successive trimming of the long-branch taxa (distance >0.19 from root in four-taxon NJ analysis) from the dataset. As would be expected²⁹, exclusion of these taxa had effects on the bootstrap support for some clades. In particular, re-analysis excluding one or all of *Panagrellus*, *Panagrolaimus*, and *Strongyloides* yielded stronger bootstrap support for the cephalobid–steinernematid clade IV (<50% to 68%), and analyses excluding the long-branch rhabditid taxa *Bumonema*, *Teratorhabditis* and *Pellioiditis* gave increased support for the Diplogasterida–Rhabditina clade V (51% to 93%). Figure 2a shows a consensus of these analyses: branchpoints that were supported by >60% in bootstrap long-branch taxa resampling of NJ or MP trees from the trimmed datasets were accepted. When there was no support for a resolved branching order, we collapsed nodes to form polytomies. Major clades supported by all analytical methods are shown and are numbered I–V. The association of Secernentea (clades II, IV and V) with the Plectidae has not been unequivocally resolved and is shown as a polytomy. We could not place the long-branch-length taxa in our trees with any certainty. We assessed statistical support for the placement of the vertebrate-parasitic taxa into four clades by calculating ML values for six-taxon subsets from the data. Each of the placements was strongly supported.

Received 16 July; accepted 12 December 1997.

- Luc, M., Sikora, R. A. & Bridge, J. *Plant Parasitic Nematodes in Tropical and Subtropical Agriculture* (CAB International, Wallingford, UK, 1990).
- Anderson, R. C. *Nematode Parasites of Vertebrates. Their Development and Transmission* (CAB International, Wallingford, UK, 1992).
- Lambhead, J. Recent developments in marine benthic biodiversity research. *Oceanis* **19**, 5–24 (1993).
- Riddle, D., Blumenthal, T., Meyer, B. & Priess, J. (eds) *C. elegans II* (Cold Spring Harbor Laboratory Press, NY, 1997).
- Ellis, R. E., Sulston, J. E. & Coulson, A. R. The rDNA of *C. elegans*: sequence and structure. *Nucleic Acids Res.* **14**, 2345–2364 (1986).
- Zarlena, D. S., Stringfellow, E., Nobary, M. & Lichtenfels, J. R. Cloning and characterisation of ribosomal RNA genes from three species of *Haemonchus* (Nematoda: Trichostrongyloidea) and identification of PCR primers for rapid differentiation. *Exp. Parasitol.* **78**, 28–36 (1994).
- Fitch, D. H. A., Bugaj-gaweda, B. & Emmons, S. W. 18S ribosomal gene phylogeny for some rhabditidae related to *Caenorhabditis elegans*. *Mol. Biol. Evol.* **12**, 346–358 (1995).
- Baldwin, J. G., Frisse, L. M., Vida, J. T., Eddleman, C. D. & Thomas, W. K. An evolutionary framework for the study of developmental evolution in a set of nematodes related to *Caenorhabditis elegans*. *Mol. Phylogenet. Evol.* **8**, 249–259 (1997).
- Baldwin, J. G. *et al.* The buccal capsule of *Aduncospiculum halicti* (Nemata: Diplogasterina): an ultrastructural and molecular phylogenetic study. *Can. J. Zool.* **75**, 407–423 (1997).
- Swofford, D. L., Olsen, G. J., Waddell, P. J. & Hillis, D. M. in *Molecular Systematics* (eds Hillis, D. M., Moritz, C. & Mable, B. K.) 407–514 (Sinauer, Sunderland, MA, 1996)
- Aguinaldo, A. M. A. *et al.* Evidence for a clade of nematodes, arthropods and other moulting animals. *Nature* **387**, 489–493 (1997).
- Lorenzen, S. *The Phylogenetic Systematics of Free-Living Nematodes* (The Ray Society, London, 1994).
- Malakhov, V. V. *Nematodes. Structure, Development, Classification and Phylogeny* (Smithsonian Institution Press, Washington, 1994).
- Maggenti, A. R. in *Concepts in Nematode Systematics* (eds Stone, A. R., Platt, H. M. & Khalil, L. F.) 25–40 (Academic, London, 1983).
- Baldwin, J. G. & Eddleman, C. D. Buccal capsule of *Zeldia punctata* (Nemata: Cephalobidae): an ultrastructural study. *Can. J. Zool.* **73**, 648–656 (1995).
- Etzinger, A. & Sommer, R. The homeotic gene *lin-39* and the evolution of nematode epidermal cell fates. *Science* **278**, 452–455 (1997).
- Poinar, G. Origins and phylogenetic relationships of the entomophilic rhabditids, *Heterorhabditis* and *Steinernema*. *Fund. Appl. Nematol.* **16**, 332–338 (1993).
- Siddiqi, M. R. Phylogenetic relationships of the soil orders Dorylaimida, Mononchida, Triplonchida and Alaimida, with a revised classification of the subclass Enoplia. *Pak. J. Nematol.* **1**, 79–110 (1983).
- Poinar, G. O. *The Natural History of Nematodes* (Prentice-Hall, Englewood Cliffs, NJ, 1983).
- De Ley, P., van de Velde, M. C., Mounport, D., Baujard, P. & Coomans, A. Ultrastructure of the stoma in Cephalobidae, Panagrolaimidae and Rhabditidae, with a proposal for a revised stoma terminology in Rhabditida. *Nematologica* **41**, 153–182 (1995).
- Winneppinnckx, B. *et al.* 18S rRNA data indicate that Aschelminthes are polyphyletic in origin and consist of at least three distinct clades. *Mol. Biol. Evol.* **12**, 1132–1137 (1995).
- Blaxter, M. L. *et al.* Genes expressed in *Brugia malayi* infective third stage larvae. *Mol. Biochem. Parasitol.* **77**, 77–96 (1996).
- Swofford, D. L. *PAUP: Phylogenetic Analysis Using Parsimony, Version 3.1* (Illinois Natural History Society, Champaign, 1993).
- Maddison, W. & Maddison, D. *MacClade v3.0* (Sinauer, Sunderland, MA, 1993).
- Kumar, S., Tamura, K. & Nei, M. *MEGA: Molecular Evolutionary Genetics Analysis. Version 1.0* (Pennsylvania State Univ., 1993).

- Van de Peer, Y., Rensing, S., Maire, U.-G. & De Wachter, R. Substitution rate calibration of small subunit subunit RNA identifies chlorarachniophyte nucleomorphs as remnants of green algae. *Proc. Natl Acad. Sci. USA* **93**, 7732–7736 (1996).
- Van de Peer, Y. & De Wachter, R. TREECON for Windows: a software package for the construction and drawing of evolutionary trees for the Microsoft Windows environment. *Comput. Appl. Biosci.* **10**, 569–570 (1994).
- Yang, Z. *Phylogenetic Analysis by Maximum Likelihood (PAML) Version 1.2* (Univ. California, Berkeley, 1996).
- Felsenstein, J. Cases in which parsimony and compatibility methods will be positively misleading. *Syst. Zool.* **27**, 401–410 (1978).

Acknowledgements. We thank our colleagues for donations of nematode material, and D. Swofford for use of prerelease versions of PAUP*4.0. This work was supported by grants from the Wellcome Trust, the Linnean Society of London, the Belgian National Fund for Scientific Research, the NSF, the NIH and the United States Department of Agriculture.

Correspondence and requests for materials should be addressed to M.L.B. (e-mail: mark.blaxter@ed.ac.uk).

Spatial and temporal organization during cardiac fibrillation

Richard A. Gray*†, Arkady M. Pertsov* & José Jalife*

* Department of Pharmacology, SUNY Health Science Center, 766 Irving Avenue, Syracuse, New York 13210, USA

† Department of Biomedical Engineering and Department of Medicine Division of Cardiovascular Disease, University of Alabama at Birmingham, 1670 University Blvd, Birmingham, Alabama 35294-0019, USA

Cardiac fibrillation (spontaneous, asynchronous contractions of cardiac muscle fibres) is the leading cause of death in the industrialized world¹, yet it is not clear how it occurs. It has been debated whether or not fibrillation is a random phenomenon. There is some determinism during fibrillation^{2,3}, perhaps resulting from rotating waves of electrical activity^{4–6}. Here we present a new algorithm that markedly reduces the amount of data required to depict the complex spatiotemporal patterns of fibrillation. We use a potentiometric dye⁷ and video imaging^{8,9} to record the dynamics of transmembrane potentials at many sites during

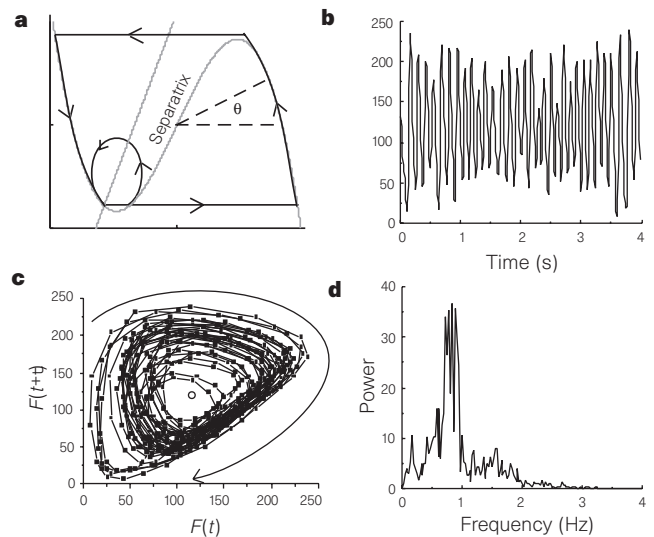


Figure 1 Temporal organization. **a**, Phase portrait of an excitable element incorporating two state variables³⁰. A stable fixed point occurs at the intersection of the nullclines (dotted lines)³⁰. **b**, Fluorescence signal (F) from a site on the surface of a rabbit heart during fibrillation. **c**, Phase portrait reveals trajectories circling around a centre (F_{mean} , F_{mean}), shown as a circle. **d**, The fluorescence signal exhibited a periodic component centred near 8 Hz, as observed in the corresponding power spectra. The frequency band 8 ± 3 Hz was different from equivalent white noise; $P < 0.00001$ for each heart (all sites combined).

fibrillation. Transmembrane signals at each site exhibit a strong periodic component centred near 8 Hz. This periodicity is seen as an attractor in two-dimensional-phase space and each site can be represented by its phase around the attractor. Spatial phase maps at each instant reveal the 'sources' of fibrillation in the form of topological defects, or phase singularities¹⁰, at a few sites. Using our method of identifying phase singularities, we can elucidate the mechanisms for the formation and termination of these singularities, and represent an episode of fibrillation by locating singularities. Our results indicate an unprecedented amount of temporal and spatial organization during cardiac fibrillation.

It is still uncertain whether rotors underlie cardiac fibrillation. Self-organized rotors giving rise to spiral waves have been observed in various excitable media¹¹⁻¹³ including cardiac muscle⁸. Although stationary spiral waves occur in isolated thin pieces of cardiac tissue, in the whole heart, as in many excitable media, they tend to move throughout the heart. If these spiral waves move rapidly (at >30% of the wave speed), they give rise to fibrillatory activity⁴. The mechanisms of cardiac fibrillation vary^{4,15}, however, and fibrillation is usually the result of multiple three-dimensional electrical waves, sometimes described as meandering wavelets, propagating throughout the heart^{16,17}. Cardiac fibrillation has been described in terms of

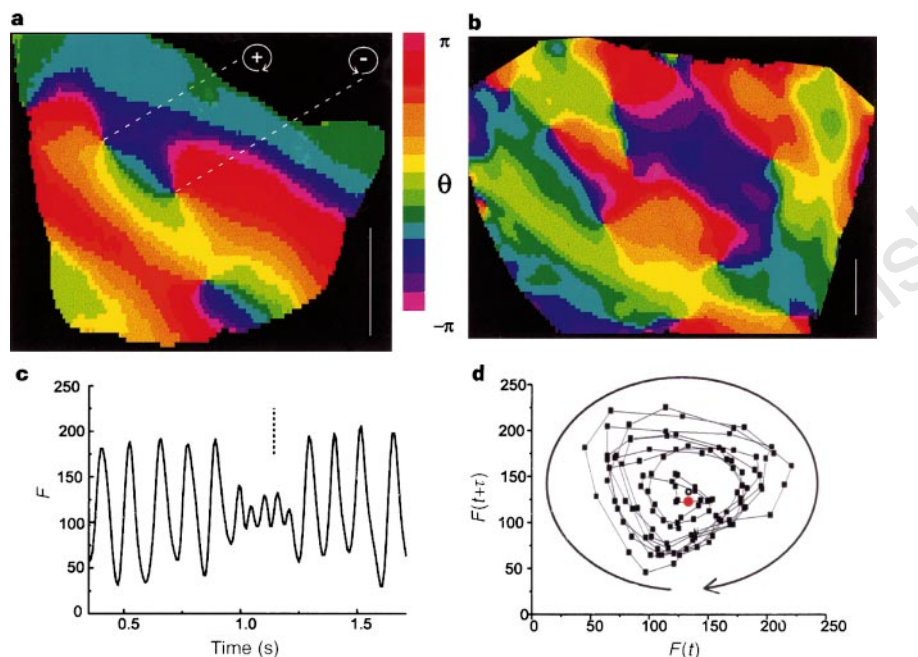


Figure 2 Snapshots of phase from the heart surface of the rabbit and sheep during sustained fibrillation. **a**, Rabbit; **b**, sheep. We classify rotor chirality as '+' for clockwise and '-' for anticlockwise²⁵. At these instants, three phase singularities (two clockwise and one anticlockwise) were observed on the rabbit heart and nine (five clockwise and four anticlockwise) on the larger sheep heart. Signals (F) demonstrate **(c)** low amplitude and **(d)** remain near the centre of their phase portraits when a spatial phase singularity site is nearby. Dashed line and red circle indicate the time of the corresponding snapshot. Vertical white line represents 1 cm.

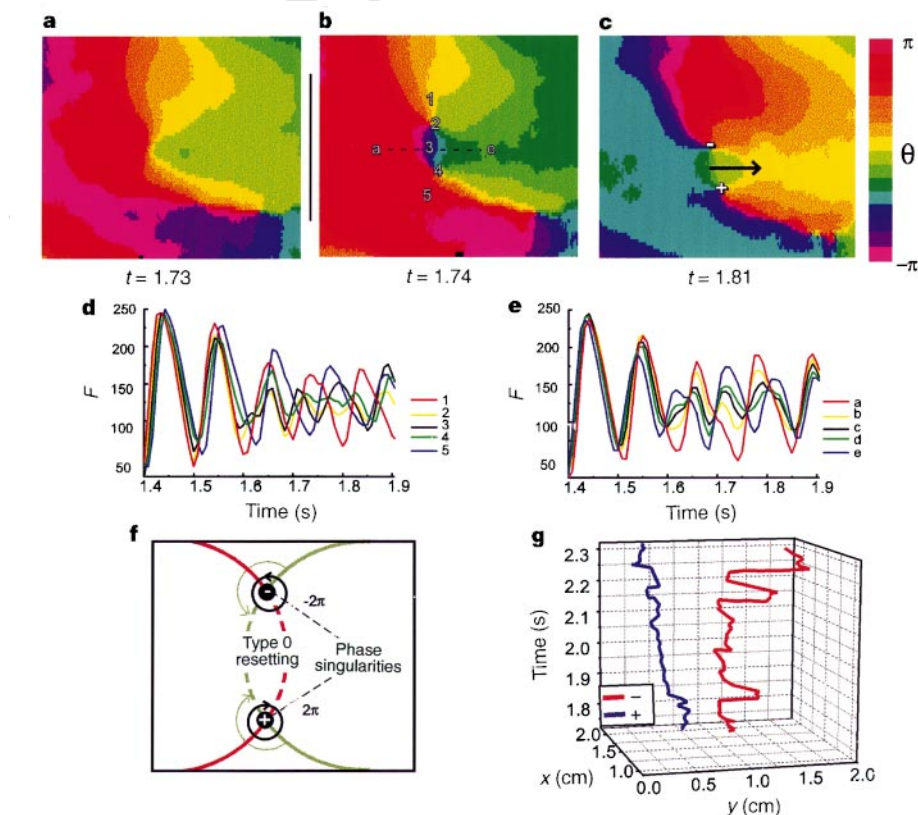


Figure 3 Initiation of a pair of spatial phase singularities. Snapshots of phase before **(a)**, during **(b)**, and after **(c)** the formation of a pair of spatial phase singularities during sustained fibrillation in the sheep heart. **d, e**, Transmembrane signals (F) measured at sites a-e and 1-5 labelled in **b, f**. A pair of singularities form when the local phase gradient becomes large (in other words, the excitation wave, $\theta \approx 0$ (green), approaches regions not fully recovered, $\theta \approx \pm \pi$ (red)). The excitation wave cannot proceed into the recovered region, and hence breaks, forming two phase singularities. The two excitation waves rotate around these newly formed singularities. Sustained rotation in the form of a pair of rotors occurs only if this excitation wave causes type 0, or even, phase resetting at the site of the initial wave break. Type 0 resetting (suprathreshold) advances the phase of this region into a new cycle, generating a new excitation wave (in the opposite direction to the previous wave; see arrow in **c**), resulting in the formation of a pair of self-sustaining rotors. Type 1 resetting (subthreshold) does not create this new excitation wave, and the phase singularity pair lasts less than one rotation. Notice the 'extra' cycle in the central region of block, sites 3 & c in **d** and **e**, indicative of type 0 resetting. **g**, Trajectories of '+' and '-' rotors following their initiation plotted in x, y, t space. Vertical line between **a** and **b** represents 1 cm.

rotors^{4-6,14,15}, on the basis of the long-held view that the heart is an example of a generic excitable medium^{10,18-20}. There are many theories about fibrillation in excitable media, but only recently have experimental techniques become available to study the complex spatial patterns observed during sustained fibrillation^{4,6,21-23}. Results from these experiments indicate that rotating waves are observed during fibrillation; however, they appear infrequently, and their initiation, termination and interaction have not been characterized.

An excitable element (for example, a cell, a patch of membrane, or a localized region in a spatially distributed system) can often be represented in phase space, which the element spends most of its time at a fixed point. A suprathreshold stimulus pushes the state of the excitable element past the separatrix and it continues along a closed-loop trajectory; however, if the stimulus is subthreshold, the state of the element does not cross the separatrix (Fig. 1). In periodic dynamics, it is simple and useful to represent the state of an element by its phase (θ) around the loop. The responses of single elements to external stimuli have been extensively studied by analysing the induced changes in θ (that is, phase resetting). Two fundamentally different responses to stimuli occur, namely, type 0 or even resetting, where a suprathreshold response gives rise to a new cycle, and type 1 or odd resetting, which effects a subthreshold response to stimuli^{10,24}. In spatially extended excitable systems, the stimulation of individual elements are provided by neighbouring elements (usually through diffusion).

A rotor is composed of a wave of excitation propagating around a topological defect, which is known as a phase singularity. A spatial phase singularity is a site in an excitable medium at which the phase of the site is arbitrary; the neighbouring elements exhibit a continuous progression of phase that is equal to $\pm 2\pi$ around this site. As shown in Fig. 1, transmembrane signals (F) recorded from the surface of rabbit and sheep hearts during fibrillation exhibited attractors in reconstructed two-dimensional phase space, when $F(t)$ was plotted against $F(t + \tau)$ where t is time and τ is the embedding delay (see Methods). Periodicity of each site was near 8 Hz. Although trajectories for subsequent cycles did not coincide in

phase space, the trajectories circulated around a central region, allowing us to construct a new variable, the phase along the attractor, θ . The phase variable (θ) calculated at each site rotated clockwise ($d\theta < 0$) 89 \pm 4% of the time, indicating that the trajectories were encircling the centre. The distance of points from the centre was smaller for $d\theta \geq 0$ compared with $d\theta < 0$ ($P < 0.0001$), as would be expected if the phase were ambiguous at the centre¹⁰. This new variable, θ , has certain advantages over the fluorescence signal (F) that simplify the analysis of fibrillation. First, use of θ eliminates the need to pick activation times, which is difficult during fibrillation, especially in the important regions of slow propagation and block. Second, we can test directly whether spatial phase singularities exist and are necessary to maintain fibrillation.

With this new method to represent fibrillation by phase, $\theta(x, y, t)$, we could study directly the detailed dynamics of spatial phase singularities and rotors, including their initiation and termination. The spatial phase patterns during sustained fibrillation (Fig. 2) concurred with theoretical predictions (for example, isophase lines connect phase singularities of opposite chirality or end on a no-flux boundary)^{10,25}. Spatial phase singularities are easily identified as sites at which all phase values ($-\pi$ to π) converge. The continuous spatial phase changes reflect waves propagating on the heart surface as a result of processes of excitation, recovery, and diffusion, and indicate that each site of the heart surface can be represented by its phase around a two-dimensional attractor. We elucidated the mechanism of rotor formation and termination by analysing successive frames of $\theta(x, y, t)$, (representative examples are shown in Figs 3 and 4). Movement of existing phase singularities created Doppler-shifted^{4,8,26} short cycle lengths, and thus created large local phase gradients in front of moving singularities. The formation of phase singularities was necessary, although not sufficient, for sustained rotation (that is, for rotor formation). In addition to the formation of phase singularities, a new excitation wave must be generated²⁷ (that is, type 0 or even resetting must occur)^{10,24} to form a rotor. Lifespan histograms for both rabbits and sheep indicate that the majority (80% for rabbit and 84% for sheep) of phase singularities lasted < 100 ms, which is less than one rotation^{4,14}. Therefore,

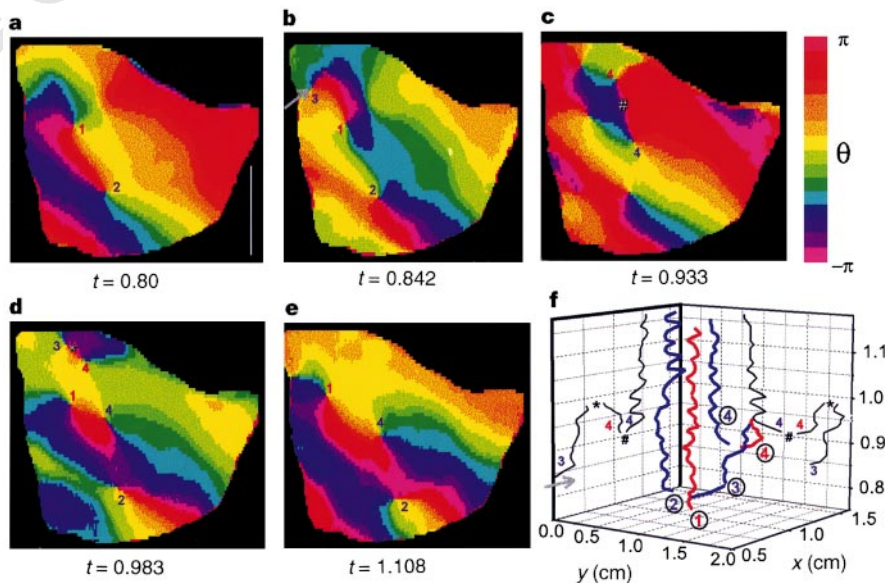


Figure 4 Dynamics of phase singularities. **a-e**, Snapshots of phase illustrating rotor dynamics on the surface of the rabbit heart during sustained fibrillation. **f**, Trajectories of the clockwise and anticlockwise rotors shown in **a-e** plotted in x, y, t space. Each rotor is numbered (1-4) and coloured (clockwise, blue; anticlockwise, red). The x and y projections in time are shown in black in **f** (except for rotors 1 and 2 for clarity). **a**, Rotors 1 and 2 formed separately before the time interval shown here (0.75-1.17 s). **b**, At $t = 0.842$ s a clockwise rotor (3) enters the

field of view from the left and moves rapidly toward the right (grey arrow in **b** and **f**). This movement creates a convergence of phase values ahead of rotor 3, and (**c**) a pair of phase singularities (4) form (# in **c** and **f**) when the excitation wave ($\theta \approx 0$) reaches the high-phase-gradient region. Both of these newly formed singularities move; the clockwise one collides with anticlockwise-rotating rotor 3, resulting in mutual annihilation (asterisk in **d**), whereas the anticlockwise one survives in the form of a rotor. Vertical white line represents 1 cm.

only ~20% of phase singularities formed rotors.

Rotor termination occurred when rotors of opposite chirality merged or when a single rotor collided with a boundary (both of these occurrences are topologically equivalent for a non-flux boundary)¹⁰. Specifically, rotor pairs were mutually annihilated if the phase gradient between the rotors, perpendicular to the line connecting the phase singularities, was sufficiently large to stop propagation. On the basis of the number of rotors observed in our recording array, each rotor occupied on average $12 \pm 4 \text{ cm}^2$. According to rough measurements of heart surface area, we estimate that the total number of rotors during fibrillation would be approximately 1–2 for rabbits, 5 for sheep, and 15 for humans (assuming the rotor density is the same in humans).

These results indicate that analysing the complex spatiotemporal patterns seen during fibrillation on the surface of the heart can be greatly simplified by identifying and analysing phase singularities. This analysis reveals topological restrictions to the dynamics of fibrillation¹⁰: first, phase lines do not intersect; second, phase singularities are joined via isophase lines to two other singularities with opposite chirality (or a boundary); and third, phase singularities form and terminate as oppositely rotating pairs (Fig. 4). Under certain conditions, phase singularities give rise to rotors, which sustain fibrillation. The direct observation of phase singularities has led, for the first time, to the quantification of fibrillation in terms of rotor number and lifespan, and to the elucidation of the mechanisms underlying the formation and termination of rotors. □

Methods

The experimental protocols, video imaging-recording system, and signal processing have been described previously^{14,28}. We acquired video images (typically 200×100 pixels) from the ventricular surface at a rate of 120 frames s^{-1} ($\Delta t = 0.00833 \text{ s}$). We applied spatial and temporal filtering to improve the signal-to-noise ratio²⁸. Two-dimensional phase portraits were obtained by plotting $F(t)$ versus $F(t + \tau)$ (ref. 29), where $t + n\Delta t$ and n is the frame number. The value of τ was chosen to be roughly one-quarter of the cycle length during fibrillation ($\tau = 25 \text{ ms}$); this value roughly corresponds to the first zero crossing of the autocorrelation of F , indicating linear independence. A new variable phase, $\theta(t)$, was computed as $\text{atan}(F(t + \tau) - F_{\text{mean}}, F(t) - F_{\text{mean}})$. Isolated hearts from rabbits of ~3 kg ($n = 3$) and from sheep of ~20 kg ($n = 3$) body weight were maintained at $36\text{--}38^\circ\text{C}$. Ventricular fibrillation was initiated by rapid pacing, and 4-s recordings were obtained at least 5 min after initiation (perfusion was maintained during fibrillation). In Figs 2–4, white and black bars near images reflect a distance of 1 cm. Values are presented as mean \pm s.d.m. Comparisons were made with paired student t -tests.

Received 30 September; accepted 8 December 1997.

- Myerburg, R. J. *et al.* in *Cardiac Electrophysiology, From Cell to Bedside* (W. B. Saunders, Philadelphia, 1990).
- Garfinkel, A. *et al.* Quasiperiodicity and chaos in cardiac fibrillation. *J. Clin. Invest.* **99**, 305–314 (1997).
- Witkowski, F. X. *et al.* Evidence for determinism in ventricular fibrillation. *Phys. Rev. Lett.* **75**, 1230–1233 (1995).
- Gray, R. A. *et al.* Mechanisms of cardiac fibrillation. *Science* **270**, 1222–1223 (1995).
- Ikeda, T. *et al.* Mechanism of spontaneous termination of functional reentry in isolated canine right atrium. *Circulation* **94**, 1962–1973 (1996).
- Lee, J. J. *et al.* Reentrant wavefronts in Wiggers' stage II ventricular fibrillation. *Circ. Res.* **78**, 660–675 (1996).
- Salzberg, B. M., Davila, H. V. & Cohen, L. B. Optical recordings of impulses in individual neurons of an invertebrate central nervous system. *Nature* **246**, 508–509 (1973).
- Davidenko, J. M., Pertsov, A. M., Salomonsz, R., Baxter, W. T. & Jalife, J. Stationary and drifting spiral waves of excitation in isolated cardiac muscle. *Nature* **355**, 349–351 (1991).
- Pertsov, A. M., Davidenko, J. M., Salomonsz, R., Baxter, W. T. & Jalife, J. Spiral waves of excitation underlie reentrant activity in isolated cardiac muscle. *Circ. Res.* **72**, 631–650 (1993).
- Winfree, A. T. *When Time Breaks Down*. (Princeton Univ. Press, 1987).
- Winfree, A. T. Scroll-shaped waves of chemical activity in three dimensions. *Science* **181**, 937–939 (1973).
- Goldbeter, A. Mechanism for oscillatory synthesis of cAMP in *Dictyostelium discoideum*. *Nature* **253**, 540–542 (1975).
- Lechleiter, J., Girdad, S. & Peralta, E. Spiral calcium wave propagation and annihilation in *Xenopus laevis* oocytes. *Science* **252**, 123–125 (1991).
- Gray, R. A. *et al.* Non-stationary vortex-like reentry as a mechanism of polymorphic ventricular tachycardia in the isolated rabbit heart. *Circulation* **91**, 2454–2469 (1995).
- Winfree, A. T. Electrical turbulence in three-dimensional heart muscle. *Science* **266**, 1003–1006 (1994).
- Moe, G. K. & Abildskov, J. A. Atrial fibrillation as a self-sustaining arrhythmia independent of focal discharge. *Am. Heart J.* **58**, 59–70 (1959).

- Allessie, M. A., Lammers, W., Bonke, F. I. M. & Hollen, J. in *Cardiac Electrophysiology and Arrhythmias* 265–275 (Grune and Stratton, Orlando, 1985).
- Krinsky, V. I. Mathematical models of cardiac arrhythmias (spiral waves). *Pharmacol. Ther.* **B 3**, 539–555 (1978).
- Zykov, V. S. *Simulation of Wave Processes in Excitable Media*. (University Press, New York/Manchester, 1987).
- Gray, R. A. & Jalife, J. Spiral waves and the heart. *Int. J. Bifurc. Chaos* **6**, 415–435 (1996).
- Bayly, P. V. *et al.* Efficient electrode spacing for examining spatial organization during ventricular fibrillation. *J. Cardiovasc. Electrophysiol.* **4**, 533–546 (1993).
- Bove, R. T. & Dillon, S. M. A new high performance system for imaging cardiac electrical activity. *Circulation* **94**, 1–714 (1996).
- Cha, Y. M., Birgersdotter-Green, U., Wolf, P. L., Peters, B. B. & Chen, P. S. The mechanism of termination of reentrant activity in ventricular fibrillation. *Circ. Res.* **74**, 495–506 (1994).
- Glass, L. & Mackay, M. C. *From Clocks to Chaos* (Princeton Univ. Press, 1988).
- Agladze, K. I. & Krinsky, V. I. Multi-armed vortices in an active chemical medium. *Nature* **296**, 424–426 (1982).
- Fast, V. G. & Pertsov, A. M. Drift of a vortex in the myocardium. *Biophysics* **35**, 489–494 (1990).
- Gotoh, M. *et al.* Cellular graded responses and ventricular vulnerability to reentry by a premature stimulus in isolated canine ventricle. *Circulation* **95**, 2141–2154 (1997).
- Gray, R. A., Ayers, G. & Jalife, J. Video imaging of atrial defibrillation in the sheep heart. *Circulation* **95**, 1038–1047 (1997).
- Takens, F. in *Dynamical Systems and Turbulence* (eds Rand, D. A. & Young, L. S.) *Lecture Notes in Mathematics* **898**, 366–381 (Springer, Berlin, 1981).
- Fitzhugh, R. Impulses and physiological states in theoretical models of nerve membrane. *Biophys. J.* **1**, 445–446 (1961).

Acknowledgements. We thank O. Berenfeld, Z. Silverman, J. Jiang and M. Flanagan for technical assistance and M. Vinson for reading the manuscript. This work was supported by grants from the Whitaker Foundation and the N.I.H.

Correspondence and requests for materials should be addressed to R.A.G. (e-mail: rag@crml.uab.edu).

Spatiotemporal evolution of ventricular fibrillation

Francis X. Witkowski*, L. Joshua Leon†, Patricia A. Penkoske‡, Wayne R. Giles§, Mark L. Spano||, William L. Ditto¶ & Arthur T. Winfree#

* Department of Medicine, and ‡ Department of Surgery, University of Alberta, Edmonton, Alberta T6G 2R7, Canada

† Ecole Polytechnique, Montreal, Quebec H3C 3J7, Canada

§ Department of Physiology and Biophysics, University of Calgary, Calgary, Alberta T2N 4N1, Canada

|| Naval Surface Warfare Center, West Bethesda, Maryland 20817, USA

¶ Applied Chaos Laboratory, School of Physics, Georgia Institute of Technology, Atlanta, Georgia 30332, USA

Department of Ecology and Evolutionary Biology, University of Arizona, Tucson, Arizona 85721, USA

Sudden cardiac death is the leading cause of death in the industrialized world, with the majority of such tragedies being due to ventricular fibrillation¹. Ventricular fibrillation is a frenzied and irregular disturbance of the heart rhythm that quickly renders the heart incapable of sustaining life. Rotors, electrophysiological structures that emit rotating spiral waves, occur in several systems that all share with the heart the functional properties of excitability and refractoriness. These re-entrant waves, seen in numerical solutions of simplified models of cardiac tissue², may occur during ventricular tachycardias^{3,4}. It has been difficult to detect such forms of re-entry in fibrillating mammalian ventricles^{5–8}. Here we show that, in isolated perfused dog hearts, high spatial and temporal resolution mapping of optical transmembrane potentials can easily detect transiently erupting rotors during the early phase of ventricular fibrillation. This activity is characterized by a relatively high spatiotemporal cross-correlation. During this early fibrillatory interval, frequent wavefront collisions and wavebreak generation⁹ are also dominant features. Interestingly, this spatiotemporal pattern undergoes an evolution to a less highly spatially correlated mechanism that lacks the epicardial manifestations of rotors despite continued myocardial perfusion.

Ventricular fibrillation is a complicated, often lethal, but poorly understood, high-frequency mode of electrical activity. It can be